AIAA JOURNAL
Vol. 49, No. 7, July 2011

Harmonic Balance Analysis of Limit Cycle Oscillations in Turbomachinery

Kivanc Ekici*
University of Tennessee, Knoxville, Tennessee 37996-2030
and
Kenneth C. Hall†
Duke University, Durham, North Carolina 27708-0300

DOI: 10.2514/1.J050858

A harmonic balance technique for the analysis of limit cycle oscillations of turbomachinery blades is presented. This method couples a computational fluid dynamics model to a single-degree-of-freedom structural dynamic model of the turbomachinery blades. The computational fluid dynamics solver uses a nonlinear frequency-domain (harmonic balance) approach that allows one to model the blade row of a turbomachine on a computational grid spanning a single blade passage. Using the harmonic balance approach, several solutions, each one corresponding to a different subtime level of the periodic unsteady flow, are computed simultaneously. These subtime-level solutions are coupled to each other in the computational field by a spectral approximation of the time-derivative term in the Navier–Stokes equation and also by application of far-field and periodic boundary conditions. The structural dynamic model is based on a similar approach in which a single vibratory mode of interest is modeled using the harmonic balance technique. The two solvers are coupled together through the upwash condition on the surface of the blade and the resulting generalized aerodynamic forces. In the proposed approach, the limit cycle oscillation frequency is treated as another unknown, which is solved iteratively, together with the governing equations of fluid flow and structural dynamics, thereby driving the residual of the aeroelastic problem to convergence in a single computational fluid dynamics run. The accuracy of the new method is compared with two other techniques and it is shown to offer significant computational savings.

Nomenclature

c	=	chord length
E	=	total energy
$\dot{f}, \dot{g}, \dot{h}$	=	control surface velocity components
I	=	rothalpy
j	=	$\sqrt{-1}$
p	=	pressure
S_t	=	Spalart–Allmaras turbulence-model source term
t	=	time
U_{inlet}	=	blade row inlet velocity
u, v, w	=	Cartesian velocities
x, y, z	=	Cartesian coordinates
x, θ, r	=	relative cylindrical coordinates
γ	=	specific heat ratio
μ_l	=	laminar viscosity
μ_t	=	turbulent viscosity
$\tilde{\nu}$	=	working turbulent variable
$\xi, \dot{\xi}$	=	amplitude and velocity of blade vibration
ρ	=	density
σ	=	interblade phase angle
τ	=	pseudotime
Ω	=	wheel speed
ω	=	excitation frequency

Presented as Paper 2010-6710 at the 46th AIAA/ASME/SAE/ASEE Joint Propulsion Conference, Nashville, TN, 25–28 July 2010; received 11 August 2010; revision received 1 February 2011; accepted for publication 9 February 2011.

*Assistant Professor, Mechanical, Aerospace and Biomedical Engineering Department. Senior Member AIAA.

†Julian Francis Abele Professor, Department of Mechanical Engineering and Materials Science. Fellow AIAA.

Introduction

ACCURATE and efficient prediction of limit cycle oscillations (LCOs) of turbomachinery blades continues to be a challenging problem because of the complex physical phenomena involved. In the literature to date [1–3], researchers have typically used time-accurate computational fluid dynamics (CFD) solvers and accompanying structural dynamic models to analyze the flutter and associated LCOs in turbomachinery. Although these methods successfully determine the aeroelastic behavior of the blades, they are relatively expensive. The computational cost is mainly associated with the cost of the time-accurate unsteady CFD solvers, which may require on the order of one to two orders of magnitude more computational time than a steady solution.

The need for more efficient and accurate unsteady flow models has led to the development of efficient nonlinear frequency-domain techniques. He and Ning [4] developed a nonlinear harmonic method to analyze unsteady flows in turbomachinery. In their approach they coupled the time-averaged flow with first-order harmonic disturbances through a deterministic stress approach. Although their unsteady analysis only considered a single harmonic, He and Ning were able to model nonlinearities in the flowfield quite accurately. A more systematic and more generalized harmonic balance (HB) method was proposed by Hall et al. [5–7] for the analysis of nonlinear unsteady flows in cascades. In recent years, Hall et al.'s harmonic balance technique was extended for the solution of a number interesting physical problems [8–16] that are temporally periodic in nature. The main advantages of the harmonic balance approach compared with a time-accurate method are its computational efficiency and its ability to more accurately model certain parts of the unsteady flow problem. For instance, the specifications of both the far-field and periodic boundary conditions are greatly simplified in the frequency domain. Complex periodicity conditions allow one to reduce the computational domain to a single blade passage in each row of a turbomachine, greatly reducing the computational cost. Furthermore, use of the pseudospectral time-derivative operator allows one to use a small number of time levels (or, equivalently, harmonics) to obtain quite accurate solutions. The resulting

equations are mathematically equivalent to steady equations and, therefore, convergence acceleration techniques used to speed convergence of steady flow solvers may be applied. On the other hand, using the time-accurate approach one marches the solution from one physical time level to the next. The size of the time step used in these computations must be small enough to ensure the stability of the flow solver. Also within each of these time steps, a number of pseudotime steps must be taken to improve the accuracy of the physical time-stepping solution, thereby increasing the computational cost. Furthermore, depending on the temporal discretization used, several solutions at previous time steps must be stored, increasing the memory requirements. These requirements make time-accurate methods somewhat less attractive compared with nonlinear harmonic technique used for time-periodic flows.

Similar to its application in CFD, the harmonic balance method can be used for the solution of a nonlinear structural system, and the frequency and amplitude of vibration that drive the coupled system to limit cycle can be determined accurately. In this paper, we investigate the LCO behavior of cascades using a dynamically nonlinear aerodynamic model and a single-degree-of-freedom nonlinear structural dynamic model, and we demonstrate the computational efficiency of the proposed coupling technique.

Unsteady Flow Solver

Governing Equations

Consider the three-dimensional Reynolds-averaged Navier–Stokes equations, with the Spalart–Allmaras [17] turbulence model to model Reynolds stresses. Written in the blade row frame of reference, which may be stationary or rotating at a speed Ω about the x axis, the governing Navier–Stokes equations are composed of five conservation equations (mass, three momentum, and energy) and one equation to represent the Spalart–Allmaras turbulence model. In Cartesian coordinates, these equations are given by

$$\frac{\partial \boldsymbol{U}}{\partial t}+\frac{\partial \boldsymbol{F}}{\partial x}+\frac{\partial \boldsymbol{G}}{\partial y}+\frac{\partial \boldsymbol{H}}{\partial z}=\boldsymbol{S} \tag{1}$$

where $\boldsymbol{U}$ is the vector of conservation variables, i.e.,

$$\boldsymbol{U}=\begin{Bmatrix}\rho\\ \rho u\\ \rho v\\ \rho w\\ \rho E\\ \rho\tilde{\nu}\end{Bmatrix}$$

The last entry, $\tilde{\nu}$, is the working variable in the Spalart–Allmaras turbulence model, from which the eddy viscosity is computed. The flux vectors $\boldsymbol{F}$, $\boldsymbol{G}$, and $\boldsymbol{H}$ and the source term $\boldsymbol{S}$ are given by

$$\boldsymbol{F}=\begin{Bmatrix}\rho u-\rho\dot{f}\\ \rho u^2+p-\tau_{xx}-\rho u\dot{f}\\ \rho uv-\tau_{xy}-\rho v\dot{f}\\ \rho uw-\tau_{xz}-\rho w\dot{f}\\ \rho uI-\tau_{xh}-\rho E\dot{f}\\ \rho u\tilde{\nu}-\tau_{xv}-\rho\tilde{\nu}\,\dot{f}\end{Bmatrix}\qquad \boldsymbol{G}=\begin{Bmatrix}\rho v-\rho\dot{g}\\ \rho uv-\tau_{yx}-\rho u\dot{g}\\ \rho v^2+p-\tau_{yy}-\rho v\dot{g}\\ \rho vw-\tau_{yz}-\rho v\dot{g}\\ \rho vI-\tau_{yh}-\rho E\dot{g}\\ \rho v\tilde{\nu}-\tau_{yv}-\rho\tilde{\nu}\,\dot{g}\end{Bmatrix}$$

$$\boldsymbol{H}=\begin{Bmatrix}\rho w-\rho\dot{h}\\ \rho uw-\tau_{zx}-\rho u\dot{h}\\ \rho vw-\tau_{zy}-\rho v\dot{h}\\ \rho w^2+p-\tau_{zz}-\rho w\dot{h}\\ \rho wI-\tau_{zh}-\rho E\dot{h}\\ \rho w\tilde{\nu}-\tau_{zv}-\rho\tilde{\nu}\,\dot{h}\end{Bmatrix}\qquad \boldsymbol{S}=\begin{Bmatrix}0\\ 0\\ \rho(\Omega^2 y+2\Omega w)\\ \rho(\Omega^2 z-2\Omega v)\\ 0\\ S_t\end{Bmatrix}$$

The shear stresses τ_{xx}, τ_{xy}, and τ_{xz} in the flux vectors are defined as

$$\tau_{xx}=\frac{2}{3}(\mu_l+\mu_t)\left(2\frac{\partial u}{\partial x}-\frac{\partial v}{\partial y}-\frac{\partial w}{\partial z}\right)$$

$$\tau_{xy}=(\mu_l+\mu_t)\left(\frac{\partial u}{\partial y}+\frac{\partial v}{\partial x}\right)\qquad \tau_{xz}=(\mu_l+\mu_t)\left(\frac{\partial u}{\partial z}+\frac{\partial w}{\partial x}\right)$$

In addition, the τ_{xh} term in the energy equation and the τ_{xv} term in the turbulence-model equation are given by

$$\tau_{xh}=\left[u\tau_{xx}+v\tau_{xy}+w\tau_{xz}+\left(\frac{\mu_l}{Pr_l}+\frac{\mu_t}{Pr_t}\right)\frac{\partial I}{\partial x}\right]$$

$$\tau_{xv}=\frac{3}{2}(\mu_l+\rho\tilde{\nu})\frac{\partial\tilde{\nu}}{\partial x}$$

The remaining components of the shear stresses and terms in energy and turbulence-model equations are defined similarly.

For an ideal gas with a constant specific heat ratio, the pressure is related to the conserved variables through

$$p=(\gamma-1)\rho[E-\tfrac{1}{2}(u^2+v^2+w^2)+\tfrac{1}{2}(\Omega r)^2]$$

Finally, the rothalpy is defined as

$$I=\frac{\rho E+p}{\rho}=\frac{\gamma}{\gamma-1}\frac{p}{\rho}+\frac{1}{2}(u^2+v^2+w^2)-\frac{1}{2}(\Omega r)^2$$

where r is the distance from the x axis ($r=\sqrt{y^2+z^2}$).

It should be noted that the inviscid flux and source vectors depend on the conservation variables, the rotational speed, and the Cartesian coordinates. The viscous fluxes depend on the gradients of the flow velocities, the temperature, and the working turbulent variable.

Harmonic Balance Approach

In this work, it is assumed that the computational turbomachinery blades vibrate harmonically with a frequency ω. The computational grid deforms to conform to this motion, so the grid also vibrates with a frequency ω about its mean position. Therefore, the flow is periodic in time, with period $T=2\pi/\omega$. Because the flow is temporally periodic, the flow variables may be represented as a Fourier series in time with spatially varying coefficients. For example, the conservation variables may be expressed as the truncated Fourier series given by

$$\boldsymbol{U}^*(x,y,z,t_i)=\boldsymbol{A}_0(x,y,z)+\sum_{n=1}^{N}[\boldsymbol{A}_n(x,y,z)\cos(\omega n t_i)+\boldsymbol{B}_n(x,y,z)\sin(\omega n t_i)];\qquad i=1{:}2N+1 \tag{2}$$

where $\boldsymbol{A}_0$, $\boldsymbol{A}_n$, and $\boldsymbol{B}_n$ are the Fourier coefficients of the conserved flow variables.

Rather than storing the Fourier coefficients, it will be convenient to store the flow variables at $2N+1$ equally spaced subtime levels over one temporal period. We denote this vector of flow variables by $\boldsymbol{U}^*$. Therefore, Eq. (2) can be written in matrix form as

$$\boldsymbol{U}^*=\mathbf{E}^{-1}\tilde{\boldsymbol{U}} \tag{3}$$

where $\mathbf{E}^{-1}$ is the inverse discrete Fourier transform operator. Conversely, the Fourier coefficients can be determined from the conservation variables by the discrete Fourier transform given by

$$\tilde{\boldsymbol{U}}=\mathbf{E}\boldsymbol{U}^* \tag{4}$$

where $\tilde{\boldsymbol{U}}$ is the vector of Fourier coefficients of the flow variables $\boldsymbol{U}^*$. Note that $\mathbf{E}$ and $\mathbf{E}^{-1}$ are square matrices, because the number of time sublevels is equal to the number of Fourier coefficients.

Next, the three-dimensional Navier–Stokes equations are expressed at all subtime levels simultaneously, so that

$$\omega \mathbf{D}\boldsymbol{U}^* + \frac{\partial \boldsymbol{F}^*}{\partial x} + \frac{\partial \boldsymbol{G}^*}{\partial y} + \frac{\partial \boldsymbol{H}^*}{\partial z} = \boldsymbol{S}^* \tag{5}$$

where, for example, $\boldsymbol{F}^*$ is the vector of x fluxes evaluated at $\boldsymbol{U}^*$. Hence, Eq. (5) has $6 \times (2N + 1)$ equations. Note that the $2N + 1$ sets of conservation equations in the field are coupled through the time-derivative term, which is approximated by the pseudospectral operator $\omega\mathbf{D}$. (The equations are also coupled through the far-field and periodic boundary conditions.)

To solve the harmonic balance equations, we introduce a pseudotime term so that the equations may be marched rapidly to a steady-state condition using a conventional computational fluid dynamic scheme [18]. Thus, Eq. (5) becomes

$$\frac{\partial \boldsymbol{U}^*}{\partial \tau} + \omega \mathbf{D}\boldsymbol{U}^* + \frac{\partial \boldsymbol{F}^*}{\partial x} + \frac{\partial \boldsymbol{G}^*}{\partial y} + \frac{\partial \boldsymbol{H}^*}{\partial z} = \boldsymbol{S}^* \tag{6}$$

where τ is a fictitious or pseudotime, used only to march Eq. (6) to steady state, driving the pseudotime term to zero. Note that pseudotime harmonic balance equations are similar in form to the original time-domain form of the Navier–Stokes equations. Thus, existing well-developed *steady* CFD techniques may be used to efficiently solve the nonlinear harmonic balance equations, with a comparable number of iterations required. Also, because only steady-state solutions are desired, local time-stepping and multiple-grid acceleration techniques are used to speed up convergence. Note that Eq. (6) is discretized on a computational grid spanning only a single blade passage, and we use Ni's [18] two-step Lax–Wendroff scheme to discretize the harmonic balance equations.

Complex Periodic Boundary Conditions

One of the advantages of the harmonic balance technique is that the computational domain can be reduced to a single blade passage by making use of complex periodicity conditions along the periodic boundaries. To apply these conditions, the solution $\boldsymbol{U}^*$ is transformed along the periodic boundaries using Eq. (4) to find the vector of Fourier coefficients $\tilde{\boldsymbol{U}}$ (which contains the cosine and sine coefficients $\boldsymbol{A}_n$ and $\boldsymbol{B}_n$). Inspection of Eq. (2) reveals that the appropriate boundary condition is given by

$$\boldsymbol{A}_n(x, r, \theta + \theta_G) = \boldsymbol{A}_n(x, r, \theta) \cdot \cos(\sigma n) + \boldsymbol{B}_n(x, r, \theta) \cdot \sin(\sigma n) \tag{7}$$

$$\boldsymbol{B}_n(x, r, \theta + \theta_G) = -\boldsymbol{A}_n(x, r, \theta) \cdot \sin(\sigma n) + \boldsymbol{B}_n(x, r, \theta) \cdot \cos(\sigma n) \tag{8}$$

where θ_G is the tangential gap for the passage, and σ is the interblade phase angle. Note that we have momentarily switched to cylindrical coordinates for simplicity.

Aeroelastic Solution Techniques

In this section we will briefly explain the structural dynamic models used in this paper for coupled aeroelastic analysis of turbomachinery blades. It is well known that the mass ratio, which is the ratio of the blade mass to the mass of the working fluid, tends to be much higher for turbomachines compared with external wings. This is mainly due to the fact that turbomachinery blades used in gas turbine engines are solid metal or nearly so. Therefore, the turbomachinery flutter, in general, occurs in a single mode (generally, at the first bending or the first torsion mode), because the aerodynamic forces are much smaller than the elastic or inertial forces, which tends to prevent modal coupling. In contrast, wing flutter generally occurs as a result of multiple mode coupling because of the low mass ratio. Thus, one can analyze, within engineering accuracy, turbomachinery linear aeroelastic phenomena considering only a single mode of vibration.

Generally, the eigenmodes and the eigenfrequencies of vibration are determined from a modal analysis of the blades. Given the mode shape and natural frequency of the blade mode of interest, the traditional time-linearized approach for the analysis of the unsteady flowfield involves enforcing the blade motion through a prescribed moving grid. Neglecting the effect of structural damping, one can then determine the stability criteria from the imaginary part of the computed generalized aerodynamic forces in the frequency domain. A negative value of the imaginary part of the generalized force corresponds to a stable system, whereas a positive value corresponds to an unstable system. To ensure the overall stability of the turbomachine, one needs to perform unsteady aerodynamic computations for each possible interblade phase angle.

Using this approach, the fluid–structure interaction can be described as one-way coupling, because the unsteady aerodynamic forces do not alter the amplitude or frequency of the structural vibration. Even with this simplifying assumption, the predictions tend to be accurate due to the high mass ratio of turbomachinery blades. The main drawback with the time-linearized unsteady solvers is their small-amplitude assumption. Therefore, they are only useful for determining the flutter onset point. In addition to the flutter onset, it is also of great interest to accurately determine the aerodynamic response to high-amplitude oscillations that may lead to limit cycle. Such problems require the use of nonlinear unsteady flow models like the time-accurate methods or the harmonic balance method. In general, unsteady flow calculations in turbomachinery using direct time simulation techniques are very expensive in terms of both computational time and memory storage. In this work a nonlinear harmonic balance technique is used for predicting the unsteady (time-periodic) aerodynamic response to blade vibrations. To analyze the overall aeroelastic characteristics, three different methods will be considered here: *prescribed-motion approach*, *Newton–Raphson coupling*, and *one-shot frequency-determination approach*.

Prescribed-Motion Approach

The first approach is based on the enforced-motion technique similar to that used in conjunction with classical time-linearized solvers. That is, for a given frequency and mode-shape pair, the aerodynamic damping (or the imaginary part of the first harmonic of the generalized force) is computed by enforcing the blade motion on the CFD grid. This method only involves unsteady aerodynamic computations and is therefore considered as a one-way coupled technique. To analyze the stability of the turbomachinery blades and to determine under which conditions limit cycle oscillations will be observed (if at all), one may need to perform HB computations for many different vibration amplitudes for each possible interblade phase angle [6,7]. The main drawback of this approach is that it is a rather brute-force method, and the overall LCO analysis may take a long time.

Newton–Raphson Coupling Approach

An improvement over the enforced-motion model is a linear structural model coupled to a nonlinear unsteady flow solver as described by Thomas et al. [19]. As mentioned before, due to the high mass ratio of the turbomachinery blades, the aeroelastic response can be determined using a single-degree-of-freedom model given by

$$m[\ddot{\xi} + 2\zeta_n \omega_n \dot{\xi} + \omega_n^2 \xi] = g \tag{9}$$

where m is the modal mass, ω_n is the natural frequency of vibration, ζ_n is the structural damping factor, and g is the generalized aerodynamic force computed using the nonlinear HB flow solver. Assuming a linear structural model [19], that is, $\xi = \bar{\xi} e^{j\omega t}$ and $g = \bar{g} e^{j\omega t}$, Eq. (9) can be converted into the frequency domain and separated into imaginary and real parts as

$$m(2\zeta_n \omega_n \omega)\bar{\xi} = \mathrm{Im}\{\bar{g}(\omega, \bar{\xi})\} \tag{10}$$

$$m(-\omega^2 + \omega_n^2)\bar{\xi} = \mathrm{Re}\{\bar{g}(\omega, \bar{\xi})\} \tag{11}$$

where $\bar{\xi}$ is the amplitude of the blade vibration and $\bar{g}$ is the first harmonic of the generalized force. Note that although the present

model considers a single harmonic to represent the blade motion, the generalized forces are determined using multiple harmonics in the HB solver. This allows one to include dynamically nonlinear aerodynamic effects due to large blade vibrations.

It should also be noted that Eq. (10) determines the stability condition of the system, whereas Eq. (11) determines the frequency of the oscillation. As can be seen, the amplitude and frequency of vibration depend on the first harmonic of the generalized force, which in fact depends on the amplitude and the frequency. Therefore, the resulting nonlinear set of equations are fully coupled. Neglecting the effect of structural damping, Eqs. (10) and (11) can be simplified to give

$$R_1(\omega, \bar{\xi}) = \mathrm{Im}\{\bar{g}(\omega, \bar{\xi})\} = 0 \tag{12}$$

$$R_2(\omega, \bar{\xi}) = \mathrm{Re}\{\bar{g}(\omega, \bar{\xi})\} - m(-\omega^2 + \omega_n^2)\bar{\xi} = 0 \tag{13}$$

which states that a neutrally stable blade vibration will take place when the imaginary part of first harmonic of the generalized force becomes zero.

As explained in Thomas et al. [19], the coupled system of equations presented above can be solved using a Newton–Raphson technique to determine the LCO frequency and the amplitude. That is,

$$\begin{Bmatrix} \omega \\ \bar{\xi} \end{Bmatrix}_{k+1} = \begin{Bmatrix} \omega \\ \bar{\xi} \end{Bmatrix}_k - \begin{bmatrix} \partial R_1/\partial\omega & \partial R_1/\partial\bar{\xi} \\ \partial R_2/\partial\omega & \partial R_2/\partial\bar{\xi} \end{bmatrix}_k^{-1} \begin{Bmatrix} R_1(\omega, \bar{\xi}) \\ R_2(\omega, \bar{\xi}) \end{Bmatrix}_k \tag{14}$$

where k is the Newton–Raphson iteration index. The Jacobian terms $\partial R_1/\partial\omega$, $\partial R_1/\partial\bar{\xi}$, $\partial R_2/\partial\omega$, and $\partial R_2/\partial\bar{\xi}$ can be determined using finite differencing. For this, at each Newton–Raphson iteration, one needs at least three converged harmonic balance solutions to compute first-order forward-difference approximations. For example,

$$\frac{\partial R_1}{\partial\omega} = \frac{R_1(\omega + \epsilon, \bar{\xi}) - R_1(\omega, \bar{\xi})}{\epsilon}$$

$$\frac{\partial R_2}{\partial\xi} = \frac{R_2(\omega, \bar{\xi} + \epsilon) - R_2(\omega, \bar{\xi})}{\epsilon}$$

where ϵ is a small number.

Note that due to the high mass ratio, the LCO frequency will be close to the natural frequency of the structure, but slightly different due to the coupled nature of the aeroelastic problem [see Eq. (13)]. If the computed value of ω is not accurate enough, the LCO condition will not be observed, i.e., the imaginary part of the first harmonic of the generalized force will not approach zero. Therefore, it is essential to carry out a sufficient number of iterations for the Newton–Raphson method. Generally speaking, the Newton–Raphson technique takes on the order of four to five iterations to determine LCO solutions to within engineering accuracy. That means the computational cost of the method can be as much as 15 times the cost of a single unsteady HB solution.

One-Shot Frequency-Determination Approach

We now turn our attention to the novel nonlinear aeroelastic method developed in this work. As explained previously, given the mode shape and the natural frequency of vibration, fully coupled aeroelastic system can be represented by a single-degree-of-freedom nonlinear mass-damper-spring equation given by Eq. (9), which is

$$m[\ddot{\xi} + 2\zeta_n\omega_n\dot{\xi} + \omega_n^2\xi] = g$$

Cast into the state-space form, Eq. (9) can be rewritten as

$$\frac{\mathrm{d}}{\mathrm{d}t}\begin{Bmatrix} \xi \\ \dot{\xi} \end{Bmatrix} + \begin{bmatrix} 0 & -1 \\ \omega_n^2 & 2\zeta_n\omega_n \end{bmatrix}\begin{Bmatrix} \xi \\ \dot{\xi} \end{Bmatrix} = \begin{Bmatrix} 0 \\ f \end{Bmatrix} \tag{15}$$

where $f = g/m$. As can be seen, Eq. (15) represents a fully coupled single-mode aeroelastic problem, which is very similar to the governing equations of fluid flow [Eq. (1)]. Therefore, Eq. (15) can be solved using a similar harmonic balance approach, so the time derivative is approximated by the pseudospectral operator $\omega\mathbf{D}$. Like the unsteady flow solution, ξ and $\dot{\xi}$ can be solved at $2N + 1$ equally spaced subtime levels over the period $T = 2\pi/\omega$. That is,

$$\omega\mathbf{D}\boldsymbol{\eta}^* + \mathbf{A}\boldsymbol{\eta}^* - \boldsymbol{R}^* = 0 \tag{16}$$

where

$$\boldsymbol{\eta}^* = \begin{Bmatrix} \xi_1 \\ \vdots \\ \xi_{2N+1} \\ \dot{\xi}_1 \\ \vdots \\ \dot{\xi}_{2N+1} \end{Bmatrix}, \qquad \mathbf{A} = \begin{bmatrix} 0\cdots0 & -1\cdots0 \\ \ddots & \ddots \\ 0\cdots0 & 0\cdots-1 \\ \omega_n^2\cdots0 & 2\zeta_n\omega_n\cdots0 \\ \ddots & \ddots \\ 0\cdots\omega_n^2 & 0\cdots2\zeta_n\omega_n \end{bmatrix}$$

$$\boldsymbol{R}^* = \begin{Bmatrix} 0 \\ \vdots \\ 0 \\ f_1 \\ \vdots \\ f_{2N+1} \end{Bmatrix}$$

Similar to the harmonic balance solution of the unsteady flow equations, one can introduce a pseudotime term so that the equations may be marched rapidly to a steady-state condition using a conventional scheme (here, we use an implicit Euler method to drive the solution to convergence). Thus, Eq. (16) becomes

$$\frac{\mathrm{d}\boldsymbol{\eta}^*}{\mathrm{d}\tau} + \omega\mathbf{D}\boldsymbol{\eta}^* + \mathbf{A}\boldsymbol{\eta}^* - \boldsymbol{R}^* = 0 \tag{17}$$

The coupled aeroelastic equation [Eq. (17)] is nonlinear because of the fact that the vector $\boldsymbol{R}^*$ contains generalized forces at different subtime levels, which are functions of modal amplitudes and velocities, as well as the frequency ω. At each iteration of the coupled problem (CFD and structural dynamics), one computes the generalized forces using the harmonic balance CFD solver, which are then used in Eq. (17) to update the values of $\boldsymbol{\eta}^*$ vector, which in turn feeds into the CFD solver. It is seen that this results in a fully coupled aeroelastic problem that drives the structural dynamic and CFD solutions to convergence at the same time.

Recall that the frequency ω of LCO is not known a priori, which contradicts the fundamental assumption of the frequency-domain CFD methods. Therefore, we need to modify the harmonic balance approach so as to predict this unknown frequency as part of the solution. In this work, we use the following idea. Suppose that the current estimate of the frequency is close to, but not precisely equal to, the LCO frequency. We may expect that if the coupled CFD/structural dynamics solution is otherwise somewhat converged, the *amplitudes* of the Fourier coefficients will be about right, but the *phase* will drift (as we will see shortly in a simple example). We therefore conclude that a reasonable estimate of the frequency is given by the frequency that minimizes the L2 norm of Eq. (17). That is to say, in the iterative process (where the values of ω, ξ, and $\dot{\xi}$ are updated at each iteration), the change in the frequency can be obtained by minimizing $\frac{1}{2}|\omega\mathbf{D}\boldsymbol{\eta}^* + \mathbf{A}\boldsymbol{\eta}^* - \boldsymbol{R}^*|^2$ at every iteration, i.e.,

$$\delta\omega = -\frac{(\boldsymbol{\eta}^{*T}\mathbf{D}^T\mathbf{A}\boldsymbol{\eta}^* - \boldsymbol{\eta}^{*T}\mathbf{D}^T\boldsymbol{R}^*)}{\boldsymbol{\eta}^{*T}\mathbf{D}^T\mathbf{D}\boldsymbol{\eta}^*} - \omega \tag{18}$$

As the value of the frequency approaches its correct value, the residual $(\omega\mathbf{D}\boldsymbol{\eta}^* + \mathbf{A}\boldsymbol{\eta}^* - \boldsymbol{R}^*)$ approaches zero, thereby satisfying

the governing equation given in Eq. (16). Note that the present technique for computing the unknown LCO frequency is similar to the gradient-based variable time period method of McMullen et al. [10]. In their approach, McMullen et al. determine the vortex-shedding frequency of a cylinder by minimizing the CFD solver residual that is rewritten as a figure of merit in an optimization problem. In our approach, we freeze the aerodynamic force f and simply use a Rayleigh quotient method to minimize the residual of the structural dynamic model.

One of the main advantages of this new coupling methodology is that it allows one to determine the conditions required for LCO in one shot, driving the residual of the aeroelastic problem to zero in a single CFD run. The convergence rate of this method will be somewhat slower than the convergence rate of a standalone CFD solution because the values of ω, ξ, and $\dot{\xi}$ need to be updated as the computation progresses. In addition, the computational time required per time step for the fully coupled solution will be 10–15% higher than that required for a standalone CFD run due to the solution of Eq. (17) and recalculation of the moving-grid terms for the updated ξ and $\dot{\xi}$ values. However, even with these added computational costs per iteration, the overall computational cost of the new method is still lower than the Newton–Raphson approach. In addition, this new technique is expected to be much more efficient than its comparable time-accurate counterparts.

Numerical Results

Nonlinear Mass-Spring-Damper System

To validate the novel aeroelastic solution technique, first consider a simple problem governed by a model nonlinear equation cast in state-space form, i.e.,

$$\frac{\mathrm{d}}{\mathrm{d}t}\begin{Bmatrix}\xi\\ \dot{\xi}\end{Bmatrix}+\begin{bmatrix}0 & -1\\ \omega_n^2 & 2\zeta_n\omega_n\end{bmatrix}\begin{Bmatrix}\xi\\ \dot{\xi}\end{Bmatrix}=\begin{Bmatrix}0\\ -\beta\dot{\xi}^3\end{Bmatrix} \tag{19}$$

Note that the above equation is essentially the same as the fully coupled nonlinear aeroelastic equation [Eq. (15)], except that the nonlinear forcing function used here is simply $-\beta\dot{\xi}^3$ instead of the generalized aerodynamic force. (Later in the paper, we will present results for which the forcing function will be the generalized aerodynamic force, leading to a fully coupled aeroelastic system.) For this example, the natural frequency of vibration is taken to be $\omega_n = 1.0$. In addition, a small structural damping, $\zeta_n = -0.1$, and cubic damping, $\beta = 1.0$, are used in computations. Since the damping of the system is small, it is known that the frequency of vibration ω that will drive the system to LCO will be very close to, but not equal to, the natural frequency.

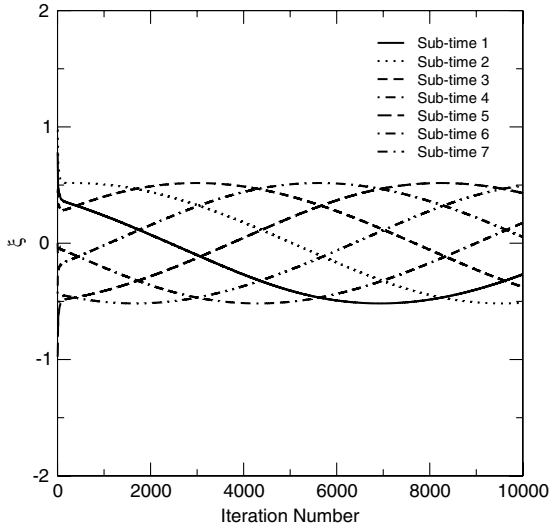

Fig. 2 Iteration number vs $\dot{\xi}$ for ω fixed at 1.0.

To demonstrate the method, we first fix the value of the excitation frequency so that $\omega = \omega_n = 1.0$ and solve Eq. (19) with three harmonics (seven subtime levels) retained in the model. Figure 1 shows ξ vs $\dot{\xi}$ at seven different subtime-level solutions as the computations progress. Within the current framework, when the excitation frequency used in the harmonic analysis is the correct value, each $(\xi, \dot{\xi})$ pair (for each subtime level) should converge to a fixed value. However, in this case it can be seen that the $(\xi, \dot{\xi})$ pairs migrate in a circle. This indicates that the harmonic solution fails to converge when ω is fixed at 1.0, although the actual LCO frequency is expected to be close to 1.0. This is more clearly seen in Fig. 2. For a converged LCO solution, the values of ξ at different subtime levels should be approaching to their fixed values, which is not the case here.

Next, starting from an initial guess of 2.0 for the LCO frequency, Eq. (19) is solved with three harmonics retained in the model, and the value of ω is updated through Eq. (18) at each iteration, minimizing the residual of the governing equation. Figure 3 shows ξ vs $\dot{\xi}$ for different subtime-level solutions. As can be seen, each subtime-level solution now converges to a fixed value as the solution progresses. The fact that the final subtime-level solutions (depicted by squares in the figure) converge to fixed values indicates that the limit cycle behavior is captured and that the frequency is accurately predicted. Note that the converged value of the LCO frequency is 0.997498 for this problem, only 0.3% different from the value of the natural frequency. Also, as can be seen in Fig. 4, the ξ values at different

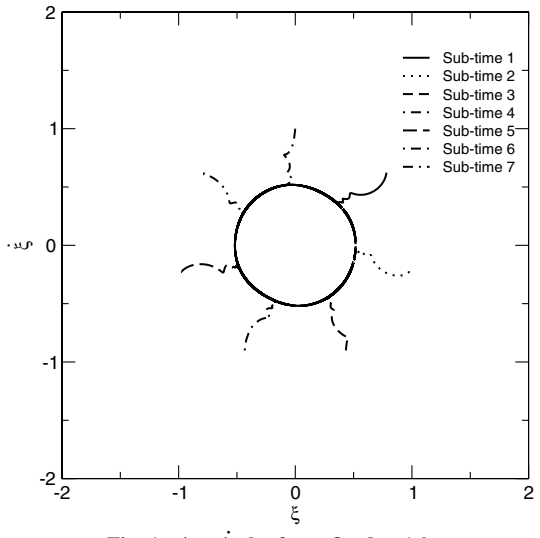

Fig. 1 ξ vs $\dot{\xi}$ plot for ω fixed at 1.0.

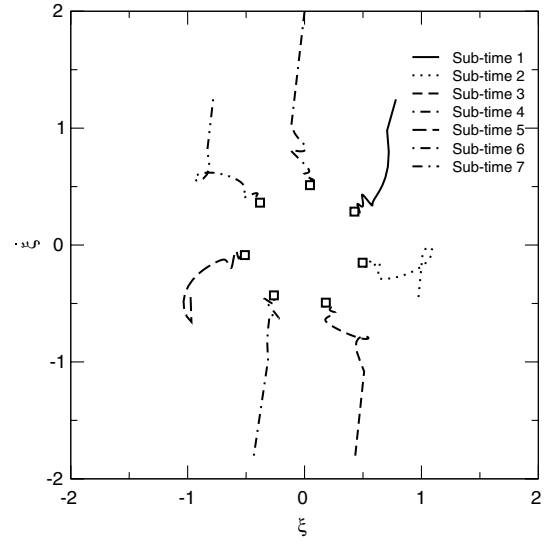

Fig. 3 LCO solution for the nonlinear spring system.

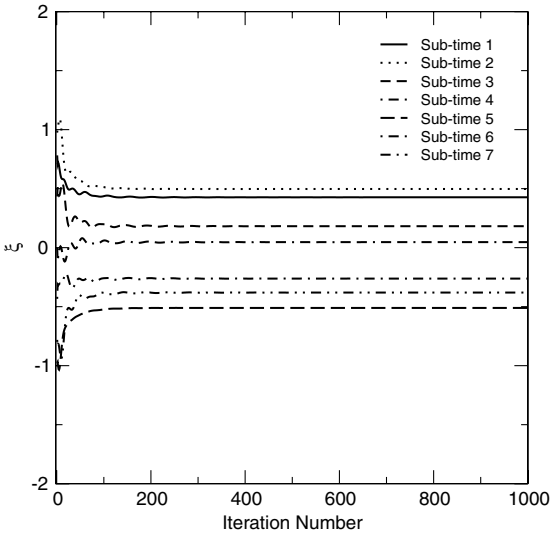

Fig. 4 Convergence of the LCO solution.

subtime levels converge to their correct values in as few as 400 iterations.

Prescribed-Motion Results

In this section, we present harmonic balance computations for unsteady flow in a two-dimensional blade section near the tip of a transonic front stage compressor blade row. Note that this case is also used and well documented in the work of Hall et al. [6,7].

At this spanwise section of the transonic rotor, the inflow Mach number is 1.27 and the inflow angle measured from the axial direction, is 59.3 deg. The geometry and the H-O-H topology grid used in this work is shown in Fig. 5. Note that although a single blade passage is used in the harmonic balance technique, the grid is shown for multiple passages for clarity. This grid consists of $193 \times 33 \times 3$ nodes in the axial, tangential, and spanwise directions, respectively. Cells in the spanwise direction are used to allow the use of our three-dimensional solver. Although not presented here, this resolution was found to produce grid-independent results.

First consider the steady flowfield in the cascade. As shown by the static pressure contours in Fig. 5, the flow structure is very interesting, with a complex shock formation in the passage. Also note that there is shock-induced boundary-layer separation aft of the strong passage shock. These results are in good qualitative agreement with those reported by Hall et al. [6]

Next, it is assumed that the blades vibrate harmonically in pitch about their midchords at a reduced frequency, $\bar{\omega} = \omega c / U_{\text{inlet}}$, of 1.0 and an interblade phase angle of 30 deg. This mode shape is somewhat representative of the first torsion mode for a typical three-dimensional rotor blade. The aerodynamic response of the rotor blades are then computed using the harmonic balance flow solver. Given the frequency and the mode shape of vibration, in the prescribed-motion method one typically performs CFD computations for a number of vibration amplitudes for all possible interblade phase angles to examine the aerodynamic response and the stability condition. To start, we assume a pitching amplitude α of 0.5 deg and determine the first harmonic of surface pressure distribution for different numbers of harmonics retained in the analysis. Shown in Fig. 6 are the real and imaginary parts of the unsteady surface pressure. As can be seen, the three- and five-harmonic solutions are in very good agreement, but are significantly different from a single-harmonic solution. Therefore, it can be said that harmonic convergence can be achieved for as few as three harmonics (or seven subtime-level solutions), and single-harmonic computations do not produce accurate results.

Having investigated the effect of the number of harmonics on the accuracy of the solution, we now compute the aerodynamic response of the blades to different pitching amplitudes. Figure 7 shows the zeroth harmonic of the surface pressure distribution for pitching amplitudes of 0.01, 0.5, and 1.0 deg. Note the small but apparent differences in the mean pressures for varying pitch amplitudes. It can be seen that as the pitch amplitude is increased, the higher harmonics in the flowfield start affecting the mean flow, which indicates a nonlinear phenomenon. In addition, it is clearly seen that as the pitching amplitude is increased, the weak shock on the suction side appears to be smeared out, which is another indication of nonlinearity.

As mentioned previously, for a one-way coupled aeroelastic model, the stability condition is determined by the imaginary part of the generalized aerodynamic force, which in turn depends on the first harmonic of the surface pressure distribution. Therefore, we now consider the unsteady surface pressure distribution for different pitch amplitudes. As shown in Fig. 8 the pressure distributions are significantly different for varying vibration amplitudes, especially in the vicinity of the shock locations. In the small-amplitude case, the so-called shock impulses (peaks of pressure) associated with the unsteady motion of the shocks are larger and narrower than in the high-amplitude cases. The fact that the unsteady shock motion has a profound effect on the unsteady pressures means that the generalized force (and hence the overall aerodynamic response) may be strongly dependent on the amplitude of the blade motion.

Finally, values of the imaginary part of the first harmonic of generalized force are presented for different values of pitch amplitude in Fig. 9. Note that the sign of the imaginary generalized force determines the stability condition for the rotor. As can be seen from the figure, the rotor is stable for pitch amplitudes greater than 0.7 deg and unstable for pitch amplitudes less than 0.6 deg. This suggests that there is a neutrally stable LCO point between 0.6 and 0.7 deg amplitude. This finding is in good agreement with what was reported by Hall et al. [7].

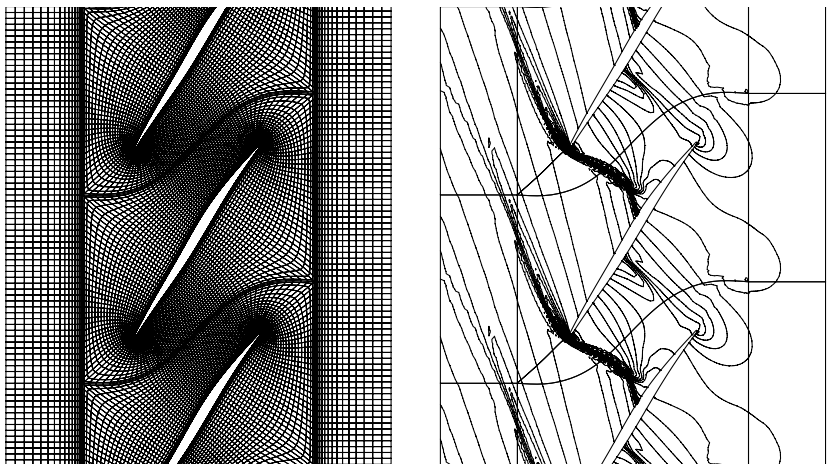

Fig. 5 Computational grid used (left) and computed static pressure contours for the transonic cascade (right). Multiple passages are shown for clarity.

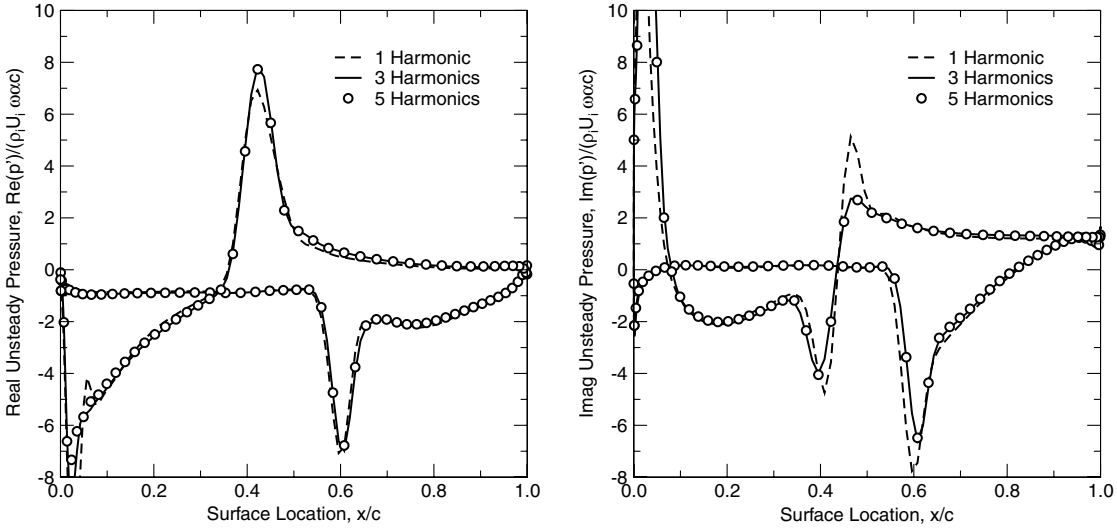

Fig. 6 First harmonic of unsteady pressure distribution on the blade surface; $\bar{\omega} = 1.0$, $\sigma = 30$ deg, and $\alpha = 0.5$ deg.

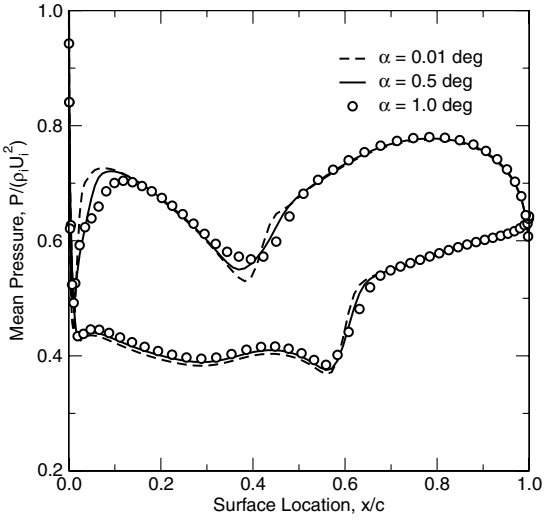

Fig. 7 Mean pressure distribution on the blade surface; $\bar{\omega} = 1.0$, $\sigma = 30$ deg, and $N = 3$ harmonics.

The results presented in this section were obtained with the assumption that the stiffness of the rotor blades is high enough that the LCO frequency is essentially the same as the natural frequency of the structure. Once the excitation frequency is known, the loosely coupled aeroelastic solution only involves prediction of the unsteady aerodynamic response at a number of mode-shape amplitudes. Of course, the prediction of the limit cycle oscillation amplitude via this method may be expensive, as it may require a large number of CFD computations.

Having determined the LCO pitch amplitude for the one-way coupled system, it is now time to turn our attention to the fully coupled solution techniques.

Newton–Raphson Coupling Results

For some cases it may be of interest to determine the aeroelastic response of a fully coupled system, where structural dynamics affect the aerodynamics and vice versa. Such cases may arise when the blade stiffness and mass are not infinitely high, so that the limit cycle frequency is different from the natural frequency of the structure. In such cases, it is required that the excitation frequency be determined as part of the solution. Because the harmonic balance technique is based on the fundamental assumption that the excitation frequency needs to be known a priori, it is necessary to devise an iterative solution technique to solve the fully coupled system. If one assumes a linear structural dynamic model with zero structural damping, the governing equation for the aeroelastic system can be written in the frequency domain [see Eqs. (12) and (13) for details] and can be solved using Newton's method, as proposed by Thomas et al. [19]. Note that the linear structural model assumption does not preclude one from using a harmonic balance technique for the solution of

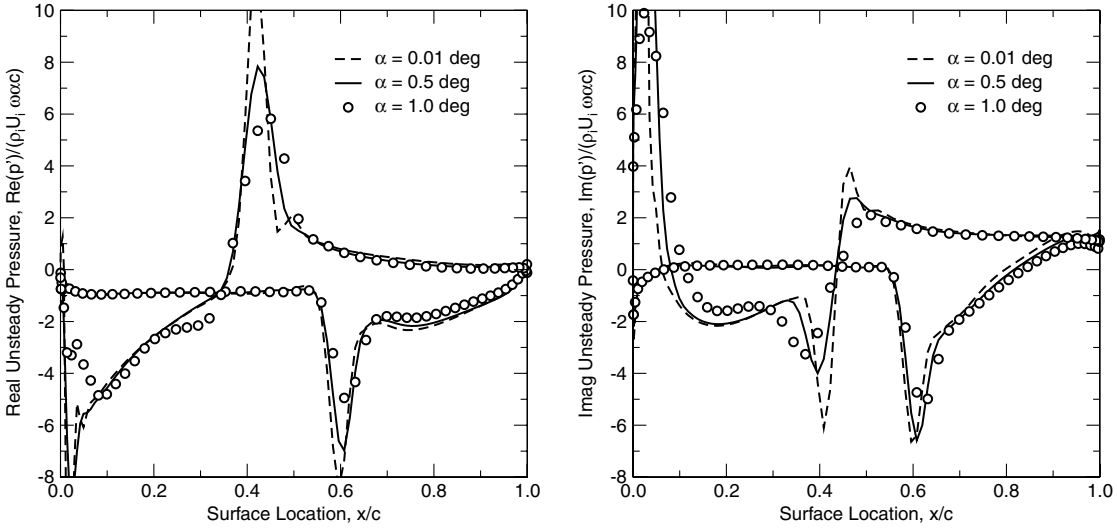

Fig. 8 First harmonic of unsteady pressure distribution on the blade surface; $\bar{\omega} = 1.0$, $\sigma = 30$ deg, and $N = 3$ harmonics.

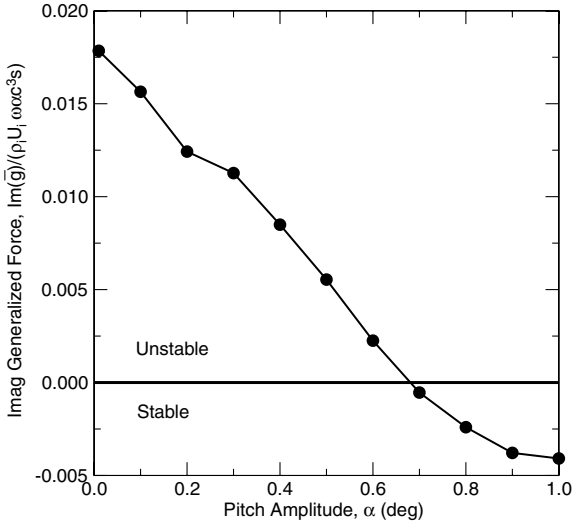

Fig. 9 Imaginary generalized force for different pitch amplitudes; $\bar{\omega} = 1.0$, $\sigma = 30$ deg, and $N = 3$ harmonics.

dynamically nonlinear flows, but rather allows one to determine the conditions that drive the system to limit cycle.

Now consider the transonic cascade case we have been investigating in this paper. The LCO solution will be found using the technique culminating in Eq. (14). To start the Newton iteration, initial guesses need to be made for the excitation frequency and the amplitude of blade vibration, which are taken to be $\omega_0/\omega_n = 1.0$ and $\bar{\xi}_0 = 0.5$ deg, where the subscript 0 corresponds to the Newton iteration index. For these initial values, the harmonic balance CFD solver is run to convergence and residuals $R_1(\omega_0, \bar{\xi}_0)$ and $R_2(\omega_0, \bar{\xi}_0)$ are computed. As explained earlier, to compute the Jacobian terms using a first-order finite difference approximation, two more converged harmonic balance computations are needed: one for $(\omega_0 + \epsilon_1, \bar{\xi}_0)$ pair and another for $(\omega_0, \bar{\xi}_0 + \epsilon_2)$, so that

$$\left.\frac{\partial R_1}{\partial \omega}\right|_0 = \frac{R_1(\omega_0 + \epsilon_1, \bar{\xi}_0) - R_1(\omega_0, \bar{\xi}_0)}{\epsilon_1};$$

$$\left.\frac{\partial R_1}{\partial \bar{\xi}}\right|_0 = \frac{R_1(\omega_0, \bar{\xi}_0 + \epsilon_2) - R_1(\omega_0, \bar{\xi}_0)}{\epsilon_2}$$

$$\left.\frac{\partial R_2}{\partial \omega}\right|_0 = \frac{R_2(\omega_0 + \epsilon_1, \bar{\xi}_0) - R_2(\omega_0, \bar{\xi}_0)}{\epsilon_1};$$

$$\left.\frac{\partial R_2}{\partial \bar{\xi}}\right|_0 = \frac{R_2(\omega_0, \bar{\xi}_0 + \epsilon_2) - R_2(\omega_0, \bar{\xi}_0)}{\epsilon_2}$$

where ϵ_1 and ϵ_2 are small numbers. The frequency and the pitching amplitude are then updated through

$$\begin{Bmatrix} \omega_1 \\ \bar{\xi}_1 \end{Bmatrix} = \begin{Bmatrix} \omega_0 \\ \bar{\xi}_0 \end{Bmatrix} - \begin{bmatrix} \partial R_1/\partial\omega|_0 & \partial R_1/\partial\bar{\xi}|_0 \\ \partial R_2/\partial\omega|_0 & \partial R_2/\partial\bar{\xi}|_0 \end{bmatrix}^{-1} \begin{Bmatrix} R_1(\omega_0, \bar{\xi}_0) \\ R_2(\omega_0, \bar{\xi}_0) \end{Bmatrix}$$

and the iterative process is repeated until convergence is achieved. The Newton–Raphson iteration convergence is presented in Table 1. As can be seen, the LCO solution converges in five Newton iterations. The first four iterations each required three unsteady flow computations. The fifth iteration, on the other hand, required only a single unsteady flow run, since the calculated imaginary generalized force was essentially zero. That means we had a total of 13 unsteady CFD runs to determine the LCO frequency and amplitude for this case. As can be seen, the predicted frequency is very close to, but not equal to, the natural frequency. In addition, the LCO pitch amplitude was predicted to be 0.677 deg, which agrees well with the computations presented in the previous section.

One-Shot Frequency-Determination Results

As the final LCO solution technique, consider the coupled nonlinear structural/nonlinear aerodynamic model developed in this work. With this proposed model, both structural dynamic and aerodynamic problems are solved using the state-of-the-art harmonic balance solution technique. As discussed previously, the harmonic balance method is based on the fundamental assumption that the frequency of excitation be known a priori, which poses a problem for fully coupled LCO solutions. This is mainly due to the fact that, although close to the natural frequency of the blades, the LCO frequency will be slightly different. Therefore, the LCO frequency needs to be treated as an unknown and must be solved iteratively together with the governing equations of fluid flow and structural dynamics. The details of this procedure can be found in the earlier parts of this paper.

The fully coupled one-shot LCO solution is started from a converged unsteady flow solution obtained for $\omega_0/\omega_n = 1.0$ and $\bar{\xi}_0 = 0.5$ deg. This unsteady solution provides a good initial guess for the coupled LCO prediction. For all computations presented in this section, three harmonics were retained in the model. First, an LCO solution was obtained for the fully coupled set of equations. Our proposed method has predicted an LCO frequency of $\omega/\omega_n = 1.000006780$ and a pitching amplitude of 0.6766383 deg. Both of these results are in excellent agreement with those presented in the previous section. Shown in Fig. 10 are the converged ξ vs $\dot{\xi}$ values for different subtime levels. Figure 11 shows the convergence of the LCO amplitude. As can be seen, the value of the amplitude does not significantly change after 10,000 iterations. Although not shown here, similar convergence was observed for the frequency prediction. In addition to monitoring the change in the pitch amplitude and the frequency (and therefore the pitch velocity), it is also necessary to check the value of the imaginary generalized force at every iteration of the solution procedure. As can be seen in Fig. 12, as the computation progresses the imaginary generalized force gradually approaches zero: the limit cycle solution.

Next, to demonstrate the importance of predicting the frequency accurately, two coupled aeroelastic computations were performed in which the excitation frequencies were fixed at $\omega = \omega_n$ and $\omega = \omega_{\text{LCO}}$. The $(\xi, \dot{\xi})$ pairs were computed for seven subtime levels. Figure 13 presents the global residual vs iteration number for the unsteady aerodynamic predictions. It is clearly seen that the fully coupled LCO solution, where the value of the excitation frequency is updated through Eq. (18), demonstrates good convergence. In addition, the coupled solution, where the excitation frequency is fixed to the LCO frequency computed from the previous run, converges at a slightly higher rate, which is to be expected. On the other hand, the computation in which the frequency is fixed at the natural frequency completely fails. These plots clearly demonstrate that to ensure convergence of the LCO solution, the value of the excitation frequency must be very accurate.

Having validated the accuracy of the proposed LCO solution technique, we now turn to the issue of computational efficiency.

Table 1 Newton–Raphson iterations for the coupled linear structural/nonlinear aerodynamic model

Iteration number	ω/ω_n	Pitch amplitude, deg	Imag. generalized force
1	1.000000000	0.5000000	$+5.547951 \times 10^{-3}$
2	1.000011305	0.8263266	-2.795822×10^{-3}
3	1.000007610	0.6797387	-7.474154×10^{-5}
4	1.000006784	0.6766270	-2.143127×10^{-6}
5	1.000006780	0.6766385	$-2.846665 \times 10^{-11}$

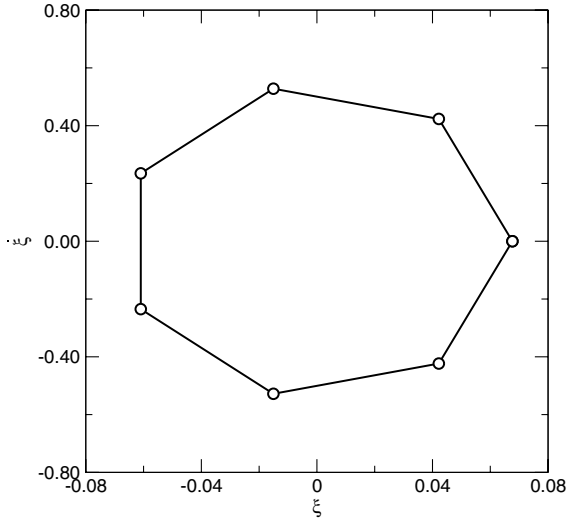

Fig. 10 Converged LCO solution for the transonic cascade.

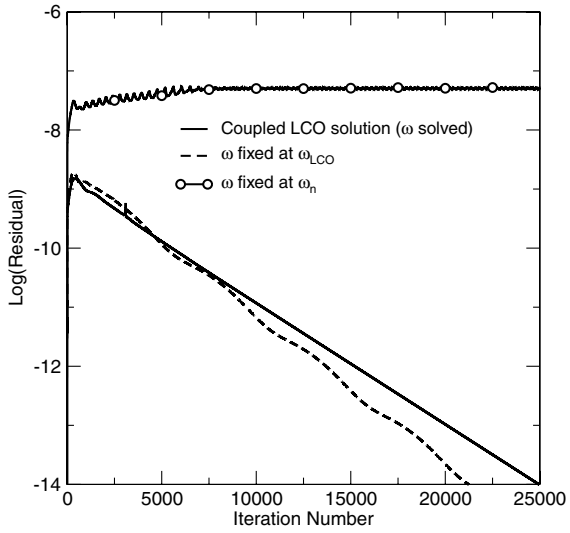

Fig. 13 Global residual vs iteration number plots for different cases.

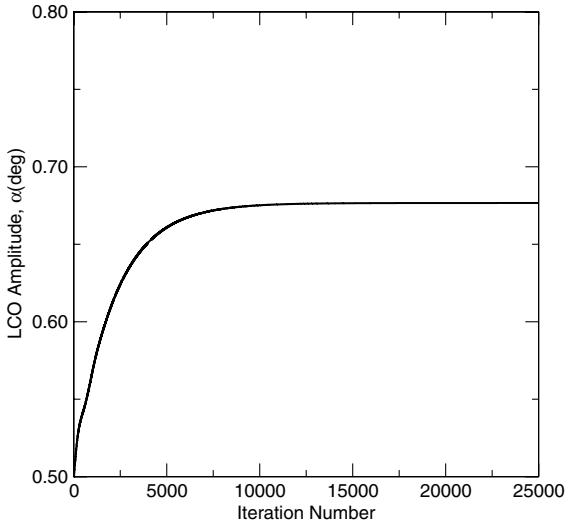

Fig. 11 LCO amplitude vs iteration number; $\sigma = 30$ deg and $N = 3$ harmonics.

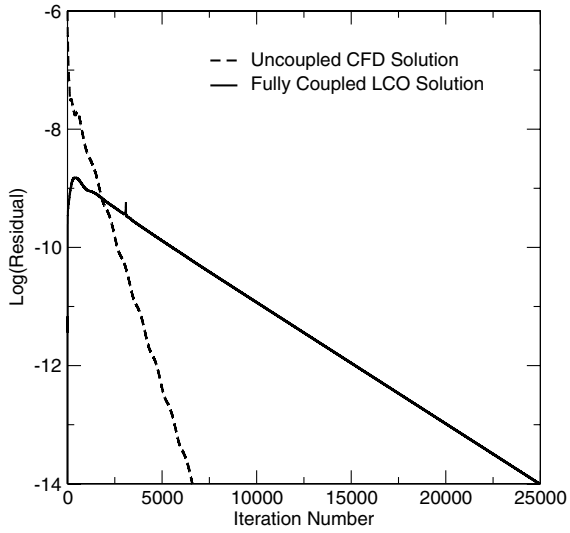

Fig. 14 Convergence histories for the LCO solution and a standalone unsteady flow solution.

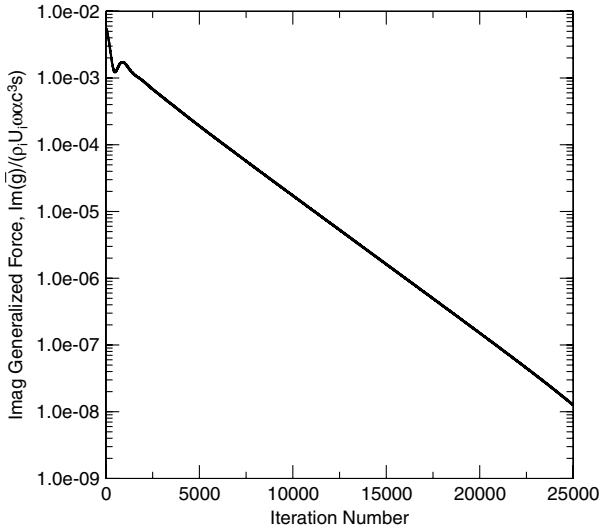

Fig. 12 Imaginary generalized force vs iteration number; $\sigma = 30$ deg and $N = 3$ harmonics.

Shown in Fig. 14 are the convergence histories for a single (uncoupled) harmonic balance CFD solution and the fully coupled one-shot aeroelastic solution. As can be seen, the new technique proposed in this work has a slower convergence rate compared with the CFD solver. The main reason for the decrease in the convergence rate is that in the aeroelastic solution, ω, ξ and $\dot{\xi}$ are updated at every iteration of the CFD solver. Overall, the fully coupled solution technique requires 3.5–4.0 times the iteration count of a single CFD solution. In addition, the fully coupled technique takes around 10–15% more CPU time per iteration. Therefore, for the case considered in this paper, the new solution technique takes around four to 5 times the computational time of a single CFD solution. By way of comparison, the Newton–Raphson method considered in this paper may take anywhere from 8 to 16 times the computational time required for a single CFD solution.

Conclusions

In this paper, a harmonic balance technique for the analysis of limit cycle oscillations of turbomachinery blades is presented. The method couples a computational fluid dynamics model to a single-degree-of-freedom structural dynamic model of the turbomachinery blades. The CFD solver uses a nonlinear frequency-domain (harmonic

balance) approach that allows one to model the blade row of a turbomachine on a computational grid spanning a single blade passage. The nonlinear structural dynamic solver is also based on harmonic balance technique. The new solution technique treats the LCO frequency as an unknown and iteratively updates its value, together with the fluid dynamic and structural dynamic equations of motion. This allows one to determine the LCO frequency and amplitude in a single run, which is demonstrated to be computationally more efficient than previous LCO prediction techniques reported in the literature.

References

[1] Doi, H., and Alonso, J. J., "Fluid/Structure Coupled Aeroelastic Computations for Transonic Flows in Turbomachinery," American Society of Mechanical Engineers, Paper GT2002-30313, 2002.

[2] Sadeghi, M., and Liu, F., "Computation of Cascade Flutter by Uncoupled and Coupled Methods," *International Journal of Computational Fluid Dynamics*, Vol. 19, No. 8, Nov. 2005, pp. 559–569.
doi:10.1080/10618560500508367

[3] Sadeghi, M., and Liu, F., "Coupled Fluid-Structure Simulation for Turbomachinery Blade Rows," AIAA Paper 2005-0018, 2005.

[4] He, L., and Ning, W., "Efficient Approach for Analysis of Unsteady Viscous Flows in Turbomachines," *AIAA Journal*, Vol. 36, No. 11, Nov. 1998, pp. 2005–2012.
doi:10.2514/2.328

[5] Hall, K. C., "Computation of Unsteady Nonlinear Flows in Cascades Using a Harmonic Balance Technique," *A Symposium in Honor of Professor Jack L. Kerrebrock's 70th Birthday*, Massachusetts Inst. of Technology, Cambridge, MA, Jan. 1998.

[6] Hall, K. C., Thomas, J. P., and Clark, W. S., "Computation of Unsteady Nonlinear Flows in Cascades Using a Harmonic Balance Technique," *9th International Symposium on Unsteady Aerodynamics, Aeroacoustics and Aeroelasticity of Turbomachines*, Lyon, France, Sept. 2000.

[7] Hall, K. C., Thomas, J. P., and Clark, W. S., "Computation of Unsteady Nonlinear Flows in Cascades Using a Harmonic Balance Technique," *AIAA Journal*, Vol. 40, No. 5, May 2002, pp. 879–886.
doi:10.2514/2.1754

[8] Chen, T., Vasanthakumar, P., and He, L., "Analysis of Unsteady Blade Row Interaction Using Nonlinear Harmonic Approach," *Journal of Propulsion and Power*, Vol. 17, No. 3, May–June 2001, pp. 651–658.
doi:10.2514/2.5792

[9] McMullen, M., Jameson, A., and Alonso, J. J., "Acceleration of Convergence to a Periodic Steady State in Turbomachinery Flows," AIAA Paper 2001-152, 2001.

[10] McMullen, M., Jameson, A., and Alonso, J. J., "Application of a Non-Linear Frequency Domain Solver to the Euler and Navier–Stokes Equations," AIAA Paper 2002-120, 2002.

[11] Thomas, J. P., Dowell, E. H., and Hall, K. C., "Modeling Viscous Transonic Limit-Cycle Oscillation Behavior Using a Harmonic Balance Approach," *Journal of Aircraft*, Vol. 41, No. 6, Nov.–Dec. 2004, pp. 1266–1274.
doi:10.2514/1.9839

[12] McMullen, M., Jameson, A., and Alonso, J., "Demonstration of Nonlinear Frequency Domain Methods," *AIAA Journal*, Vol. 44, No. 7, 2006, pp. 1428–1435.
doi:10.2514/1.15127

[13] Vilmin, S., Lorrain, E., Hirsch, C., and Swoboda, M., "Unsteady Flow Modeling Across the Rotor/Stator Interface Using the Nonlinear Harmonic Method," American Society of Mechanical Engineers, Paper GT2006-90210, 2006.

[14] Gopinath, A., van der Weide, E., Alonso, J. J., Jameson, A., Ekici, K., and Hall, K. C., "Three-Dimensional Unsteady Multi-Stage Turbomachinery Simulations Using the Harmonic Balance Technique," AIAA Paper 2007-0892, 2007.

[15] Ekici, K., Hall, K. C., and Dowell, E. H., "Computationally Fast Harmonic Balance Methods for Unsteady Aerodynamic Predictions of Helicopter Rotors," *Journal of Computational Physics*, Vol. 227, No. 12, 2008, pp. 6206–6225.
doi:10.1016/j.jcp.2008.02.028

[16] Ekici, K., and Hall, K. C., "Nonlinear Frequency-Domain Analysis of Unsteady Flows in Turbomachinery with Multiple Excitation Frequencies," *AIAA Journal*, Vol. 46, No. 8, Aug. 2008, pp. 1912–1920.
doi:10.2514/1.26006

[17] Spalart, P. R., and Allmaras, S. R., "One-Equation Turbulence Model for Aerodynamic Flows," AIAA Paper 92-0439, 1992.

[18] Ni, R. H., "A Multiple-Grid Scheme for Solving the Euler Equations," *AIAA Journal*, Vol. 20, No. 11, Nov. 1982, pp. 1565–1571.
doi:10.2514/3.51220

[19] Thomas, J. P., Dowell, E. H., and Hall, K. C., "Nonlinear Inviscid Aerodynamic Effects on Transonic Divergence, Flutter, and Limit-Cycle Oscillations," *AIAA Journal*, Vol. 40, No. 4, April 2002, pp. 638–646.
doi:10.2514/2.1720

A. Sinha
Associate Editor